Proceedings of the Geologists' Association 123 (2012) 74–86

Contents lists available at ScienceDirect

Proceedings of the Geologists' Association

journal homepage: www.elsevier.com/locate/pgeola

Review paper

Seismic interferometry and ambient noise tomography in the British Isles

Heather Nicolson [a,b,c], Andrew Curtis [a,b,*], Brian Baptie [b,c], Erica Galetti [a,b]

[a] School of GeoSciences, University of Edinburgh, Grant Institute, West Mains Rd., Edinburgh EH9 3JW, UK
[b] ECOSSE (Edinburgh Collaborative of Subsurface Science and Engineering), UK
[c] British Geological Survey, Murchison House, Kings Buildings, West Mains Road, Edinburgh, UK

ARTICLE INFO

Article history:
Received 10 September 2010
Received in revised form 1 April 2011
Accepted 1 April 2011
Available online 10 May 2011

Keywords:
Seismic interferometry
Ambient noise tomography
Surface waves
Scottish Highlands

ABSTRACT

Traditional methods of imaging the Earth's subsurface using seismic waves require an identifiable, impulsive source of seismic energy, for example an earthquake or explosive source. Naturally occurring, ambient seismic waves form an ever-present source of energy that is conventionally regarded as unusable since it is not impulsive. As such it is generally removed from seismic data and subsequent analysis. A new method known as seismic interferometry can be used to extract useful information about the Earth's subsurface from the ambient noise wavefield. Consequently, seismic interferometry is an important new tool for exploring areas which are otherwise seismically quiescent, such as the British Isles in which there are relatively few strong earthquakes. One of the possible applications of seismic interferometry is ambient noise tomography (ANT). ANT is a way of using interferometry to image subsurface seismic velocity variations using seismic (surface) waves extracted from the background ambient vibrations of the Earth. To date, ANT has been used successfully to image the Earth's crust and upper-mantle on regional and continental scales in many locations and has the power to resolve major geological features such as sedimentary basins and igneous and metamorphic cores. Here we provide a review of seismic interferometry and ANT, and show that the seismic interferometry method works well within the British Isles. We illustrate the usefulness of the method in seismically quiescent areas by presenting the first surface wave group velocity maps of the Scottish Highlands using only ambient seismic noise. These maps show low velocity anomalies in sedimentary basins such as the Moray Firth, and high velocity anomalies in igneous and metamorphic centres such as the Lewisian complex. They also suggest that the Moho shallows from south to north across Scotland which agrees with previous geophysical studies in the region.

Contents

1. Introduction

Over the last decade, a new method known as seismic or wavefield interferometry has revolutionised passive seismology. Traditionally, seismologists analyse waves from earthquakes or

* Corresponding author at: School of GeoSciences, University of Edinburgh, Grant Institute, West Mains Rd., Edinburgh EH9 3JW, UK.
E-mail addresses: h.j.nicolson@gmail.com (H. Nicolson), Andrew.Curtis@ed.ac.uk (A. Curtis), bbap@bgs.ac.uk (B. Baptie), E.Galetti@sms.ed.ac.uk (E. Galetti).

0016-7878/$ – see front matter © 2011 The Geologists' Association. Published by Elsevier Ltd. All rights reserved.
doi:10.1016/j.pgeola.2011.04.002

artificial energy sources that travel through the Earth, in order to make inferences about Earth's subsurface structure and properties. However ambient seismic noise – seismic waves caused by wind, ocean waves, rock fracturing and anthropogenic activity – also constantly travel through the Earth. Somewhere within its complex wavefield, ambient seismic noise must also contain similar information about the Earth's subsurface.

Typically, however, much time and effort is invested in removing this contaminating "noise" from seismic data in order to enhance coherent signals. This is because until around 2003 it was not known how to extract the useful subsurface information from the noise. The emergence of seismic interferometry theory (e.g. Wapenaar, 2003, 2004; Campillo and Paul, 2003; van-Manen et al., 2005, 2006, 2007; Wapenaar and Fokkema, 2006; Slob et al., 2007; Curtis et al., 2009; Curtis and Halliday, 2010a,b; Wapenaar et al., 2011) allowed us to decode the information contained in the ambient noise wavefield to create a useful signal, in fact an artificial seismogram, from what used to be called noise. This new seismogram can then be used to image the subsurface of the Earth using traditional seismological tomographic or imaging methods.

The field of wavefield interferometry has developed between the domains of physics, acoustics and geophysics, although within the geophysics community it is commonly referred to as seismic interferometry. The use of wavefield or seismic interferometry has increased greatly in recent years and in this time has been applied in many novel ways to retrieve useful signals from background noise sources (e.g. Rickett and Claerbout, 1999; Lobkis and Weaver, 2001; Weaver and Lobkis, 2001; Campillo and Paul, 2003; Shapiro and Campillo, 2004; Sabra et al., 2005a,b; Shapiro et al., 2005; Yang et al., 2006; Draganov et al., 2006; Bensen et al., 2007, 2008; Yang et al., 2008; Yang and Ritzwoller, 2008; Zheng et al., 2008) and active or impulsive sources (e.g. Bakulin and Calvert, 2006; Slob et al., 2007; Lu et al., 2008; King et al., 2010), for computing or modelling synthetic waveforms (van-Manen et al., 2005, 2006, 2007), and for noise prediction and removal from data (Curtis et al., 2006; Dong et al., 2006; Halliday et al., 2007, 2008, 2010; Halliday and Curtis, 2008, 2009).

Ambient noise tomography (ANT), a method of using interferometry to image subsurface seismic velocity variations using seismic (surface) waves extracted from the background ambient vibrations of the Earth, allows us to uncover new information about the Earth which is difficult to achieve with traditional seismic methods. For example, stable continental interiors tend to be seismically quiet. If sufficient ambient seismic noise propagates through such an area however, ANT offers us the opportunity to image the Earth's shallow subsurface which would otherwise be difficult to accomplish using local earthquake tomography methods. Some of the most interesting continental regions on Earth are covered by vast areas of water, for example Hudson Bay in Canada. Again, ANT allows us to record information about the subsurface of such areas without the need for expensive ocean-bottom seismometer equipment (e.g. Pawlak et al., 2010). To date, surface wave components of inter-receiver Green's functions have been most successfully reconstructed from ambient seismic noise. Fortunately, many established methods to analyse seismic surface waves are already widely used by surface-wave seismologists. In addition, ANT might be utilized as an important reconnaissance method, preceding more detailed study of an area using traditional controlled or passive source methods.

In this paper we review the theory of seismic interferometry and in particular ambient noise tomography. We then show that artificial or "virtual" seismograms can be constructed using noise propagating across southern England. Finally we apply this method to the Scottish Highlands to demonstrate the usefulness of this approach in seismically quiescent areas, such as the British Isles. Earthquakes do occur in Scotland, but they tend to be infrequent and of small magnitude (Baptie, 2010). Our extensive knowledge of the surface geology of Scotland provides us with many important constraints on its tectonic evolution. However, a lack of local earthquake tomography and detailed wide-angle seismic studies in the region means that its crustal seismic velocity structure is not particularly well constrained compared to some other continental regions. In addition, until the early 2000s only a small number of broadband seismometers were located in Scotland leading to poor station coverage for detailed tomographic studies. Here we apply ANT to a dense, continuously recording network of broadband seismometers that cross many of the major tectonic and terrane boundaries in Scotland. In so doing we traverse approximately 2 billion years of the geological record, from Precambrian basement, through the Caledonian orogeny to Tertiary volcanism associated with the opening of the North Atlantic.

1.1. Historical background

The basic idea of the seismic interferometry method is that the so-called Green's function between two seismic stations (seismometers) can be estimated by cross-correlating long time series of ambient noise recorded at the stations. A Green's function between two points may be thought of as the seismogram recorded at one location due to an impulsive or instantaneous source of energy at the other. The importance of a Green's function is that it contains information about how energy travels through the Earth between the two locations. Traditional seismological methods extract such information to make inferences about the Earth's subsurface.

Claerbout (1968) proved that it was possible to construct the Green's function from one point on the Earth's surface back to itself (i.e. the Green's function describing how energy travels down into the Earth's subsurface from a surface source, and then reflects back to the same point on the surface) without ever using a surface source. Instead, the Green's function could be constructed by cross-correlating a seismic wavefield that has travelled from an energy source deep in the subsurface to the same point on the Earth's surface with itself. Claerbout's conjecture, that the same process would work to create seismograms between any two points on or inside the three-dimensional Earth, remained intriguing and unproven for more than twenty years.

The idea was revisited in 1988 when Cole (1988, 1995) attempted to validate Claerbout's conjecture using a dense array of passively recording geophones on the Stanford University campus. Unfortunately Cole was unsuccessful in observing the reflected waves from cross-correlations across the array. The first demonstration of Claerbout's conjecture occured in 1993, although somewhat unexpectedly on the Sun rather than the Earth. Duvall et al. (1993) showed that "time-versus-distance" seismograms can be computed between pairs of locations on the Sun's surface by cross-correlating recordings of solar surface noise at a grid of locations measured with the Michelson Doppler Imager. Rickett and Claerbout (1999) summarised the application of noise cross-correlation in helioseismology and thus conjectured for the Earth that "by cross-correlating noise traces recorded at two locations on the surface, we can construct the wave-field that would be recorded at one of the locations if there was a source at the other" (Rickett and Claerbout, 1999). The conjecture was finally proven mathematically by Wapenaar (2003, 2004), Snieder (2004) and van-Manen et al. (2005) for acoustic media, by van-Manen et al. (2006) and Wapenaar and Fokkema (2006) for elastic media, and was demonstrated in laboratory experiments by Lobkis and Weaver (2001), Weaver and Lobkis (2001), Derode et al. (2003) and Larose et al. (2005). Thereafter these methods became common practise in seismology. The first empirical seismological demonstrations were achieved by Campillo and Paul (2003),

Shapiro and Campillo (2004) and Sabra et al. (2005a) who showed that by cross-correlating recordings of a diffuse seismic noise wavefield at two seismometers, the resulting cross-correlogram approximates the surface wave components of the Green's function between the two receivers as if one of the receivers had actually been a source. Surface waves travel around the Earth trapped against the surface but vibrating throughout the crust and mantle. It is these waves that are now usually synthesised and analysed by seismic interferometry studies.

2. Theory and method of seismic interferometry

The theory behind interferometry is relatively straightforward to understand and apply. Consider the situation shown in Fig. 1a. Two receivers (e.g. seismometers) at positions $\mathbf{r}_1$ and $\mathbf{r}_2$ are surrounded by energy sources located on an arbitrary surrounding boundary **S**. The wavefield emanating from each source propagates into the medium in the interior of **S** and is recorded at both receivers. The signals recorded at the two receivers are then cross-correlated. If the cross-correlations from all of the sources are subsequently stacked (added together), the energy that travelled along paths between $\mathbf{r}_1$ and $\mathbf{r}_2$ will add constructively, whereas energy that did not travel along these paths will add destructively. Hence, the resulting signal will approximate the Green's function between $\mathbf{r}_1$ and $\mathbf{r}_2$, as if one of the receivers had actually been a source (Fig. 1b) (Wapenaar, 2003, 2004). We therefore refer to this Green's function as a seismogram from a "virtual" (imaginary) source at the location of one of the receivers ($\mathbf{r}_1$).

The above is for the case where each source is fired sequentially and impulsively. For the case of random noise, one can imagine that a surface **S** exists such that it joins up all of the noise sources. Since noise sources may all fire at the same, or at overlapping times, their recorded signals at the two receivers are already summed together, hence the stacking step above has already taken place quite naturally. As shown by Wapenaar (2004) for acoustic media, and by van-Manen et al. (2006) and Wapenaar and Fokkema (2006) for elastic media, the inter-receiver Green's function is approximated by the cross-correlation of the noise recordings provided that the noise sources themselves are uncorrelated (i.e. they are independent of each other), the surface **S** is large (far from the two receivers), certain conditions on the type of noise sources are met, and that the noise is recorded for a sufficiently long time period. While it is usually unclear whether all of these conditions are met in practise, experience shows that the results are nevertheless useful.

In the early applications of seismic interferometry it was recognised that two key conditions of the method were that the wave-fields must be diffuse i.e. waves should propagate from all directions equally, and hence that the sources should entirely surround the medium of interest (Weaver and Lobkis, 2002), and that both monopolar (e.g. explosive, pressure or displacement) and dipolar (e.g. strain) sources were required on the boundary. Therefore the path to using ambient seismic noise for seismic interferometry was not immediately obvious since the ambient wave-field is not diffuse, the distribution of noise sources around any boundary **S** tends to be inhomogeneous, and there is no guarantee that the sources are of both monopolar and dipolar nature. Nevertheless, Campillo and Paul (2003), Shapiro and Campillo (2004) and Sabra et al. (2005a) showed that surface waves, in particular Rayleigh waves (a type of seismic surface wave), could be obtained by cross-correlating ambient seismic noise across the United States. The two conditions of the method can be relaxed for the ambient noise field given first that a long time period of noise can be used, for example a year or more, and second that waves scatter in a very complex manner in the Earth's crust. Thus the azimuthal distribution of recorded noise will tend to homogenise (Campillo and Paul, 2003; Yang and Ritzwoller, 2008). Snieder (2004) also showed that the seismic sources located around the extensions of the inter-receiver path (Fig. 1c) contribute most to the interferometric Green's function construction, and so a whole boundary of sources is not necessary in order to approximate the inter-receiver Green's function. Finally, Wapenaar and Fokkema (2006) showed that the Green's function could also be approximated using only monopolar sources, provided that these were distributed randomly in space (i.e. provided that the boundary *S* is rough), or provided that they were (i.e. boundary *S* was) sufficiently far from either receiver.

Since passive seismic interferometry relies on the geometry of seismic receiver locations only, and requires no impulsive sources like earthquakes in order to obtain useful seismograms (Green's functions), the technique is particularly useful in seismically quiescent areas, for example within the British Isles. Fig. 2 shows a comparison between real Rayleigh waves from a British earthquake recorded at a British seismometer and Rayleigh waves extracted purely from ambient noise by interferometry along approximately the same path of propagation. A seismogram from the $M_L = 4.2$ Folkestone earthquake in April 2007 was recorded at station CWF, approximately 246 km away in central England (Fig. 2a and b). The Rayleigh waves arrive between 80 s and 120 s after the earthquake's origin time. Soon thereafter, the British Geological Survey installed station TFO very close (~5 km) to the epicentre in order to monitor the aftershock sequence (Fig. 2a). Fig. 2c shows 5–10 s period Rayleigh waves synthesised by cross-correlating three months (June, July and August 2007) of noise

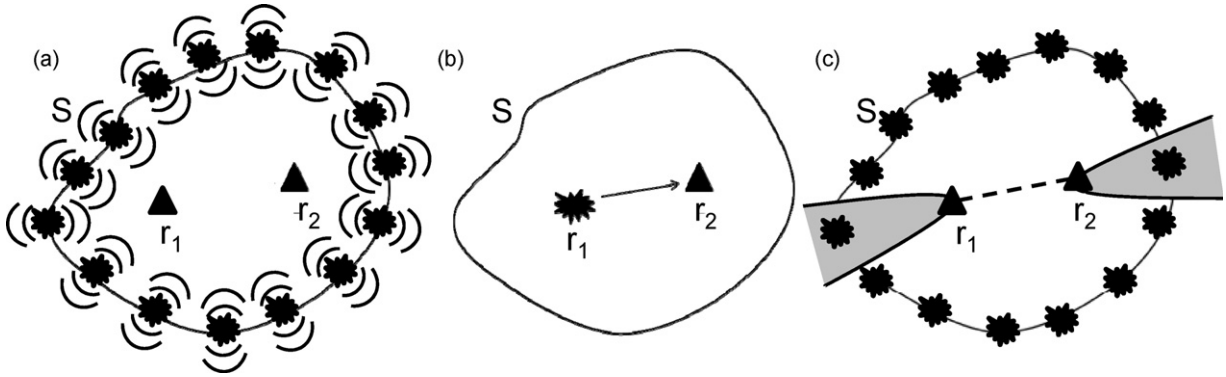

Fig. 1. A schematic explanation of the seismic interferometry method. (a) Two receivers (triangles) are surrounded by a boundary *S* of sources (explosions), each of which sends a wavefield into the interior and exterior of *S* (wavefronts shown). (b) The seismic interferometry method turns one of the receivers ($\mathbf{r}_1$) into a virtual source from which a real seismogram is obtained. (c) Sources located within the grey regions contribute the most to the Green's function computation.

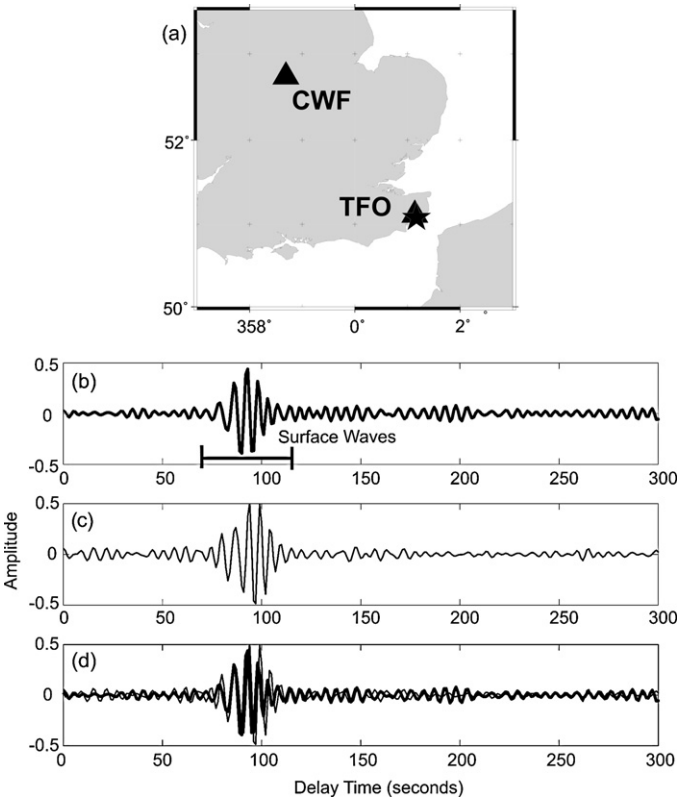

Fig. 2. (a) Location map showing stations CWF and TFO (triangles) and the epicentre of the Folkestone earthquake (star); (b) real earthquake recording at CWF (the horizontal bar indicates the surface (Rayleigh) wave energy); (c) cross-correlation between three months of ambient noise recorded by seismometers at TFO and CWF; (d) comparison of waveforms in (b) and (c). All waveforms are band-pass filtered between 5 and 10 s. The Rayleigh waves arrive between 80 and 120 s after the earthquake occurred.

recordings at TFO and CWF. The real 5–10 s period Rayleigh waves from the Folkestone earthquake recorded at CWF shown in Fig. 2b are compared directly with the seismogram constructed from ambient or background noise alone in Fig. 2d. The real and synthesised waves are not exactly the same since the earthquake focus and station TFO are not co-located, the earthquake is itself not exactly impulsive (the rupture takes a significant time to occur) and due to the other theoretical approximations described above. Nevertheless, the similarity between the two seismograms is clear, showing that within the United Kingdom we can obtain *real* seismograms from *virtual* energy sources using only recordings of background ambient seismic noise.

The surface-wave parts of inter-receiver Green's functions appear particularly clearly in seismograms constructed from seismic interferometry. This is because strong sources of seismic noise are in general restricted to locations within or on the Earth's crust. Surface waves travel along the interfaces between different layers; within the Earth, they propagate particularly strongly within the crust and upper-mantle. Seismic surface waves can divide into Love waves which have transverse horizontal vibrations (perpendicular to the direction of propagation), and Rayleigh waves which have longitudinal (parallel to the direction of propagation) and vertical motion. Both of these types of surface waves are observable on cross-correlations of ambient seismic noise in the British Isles (Fig. 3).

3. Ambient noise tomography

One particularly useful property of surface waves is that they are dispersive: the longer period waves within a packet of surface

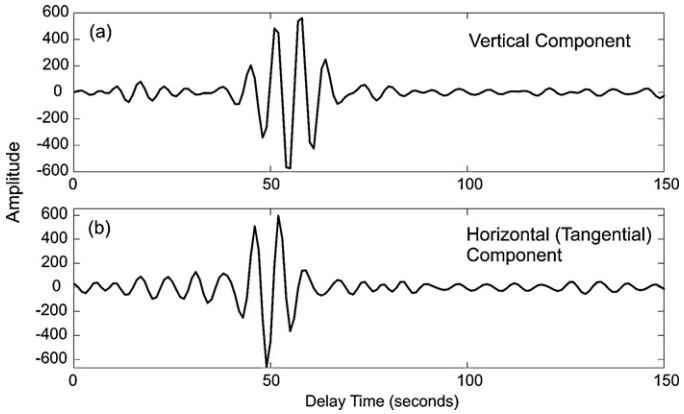

Fig. 3. 5–10 s period (a) Rayleigh and (b) Love surface waves between seismometers, separated by approximately 165 km, at MILN (near Kinross, Perthshire) and KYLE (near Skye, Scottish Highlands) (Fig. 6) constructed from a year of ambient seismic noise.

wave energy have a longer wavelength and hence penetrate deeper into the Earth. Given that seismic velocity generally increases with depth, these longer period waves usually travel faster than the shorter period, and hence shorter wavelength surface waves since these are sensitive to the seismically slower velocities at shallower depths. On a seismogram, it is therefore normal to observe long period surface waves arriving earlier than short period surface waves (Fig. 4 – top). Surface wave dispersion can be represented as a dispersion curve, which is a plot of the speed of travel of a surface wave versus period. For example Fig. 5 shows typical surface wave velocity dispersion curves for average continental crust. By separating an observed surface wave seismogram, either real or interferometric, into individual periods or equivalently frequencies (typically by applying a narrow band-pass filter centred on each target frequency), we can measure the speed with which energy at each frequency has travelled between an earthquake or a virtual source and a receiver (Fig. 4).

Since different frequencies are sensitive to properties at different depths, study of surface wave dispersion allows us to infer information about how seismic velocity varies with depth in the Earth (e.g. Dziewonski et al., 1969, 1972). Typically, periods below about 20 s are mainly sensitive to crustal structure and properties, and above 20 s are also sensitive to properties of the upper mantle. Inverting surface wave velocities at different periods, measured for many paths within a given region, to obtain models of the Earth's velocity structure with depth is known as surface wave tomography.

In the first applications of surface wave tomography using interferometric surface waves from ambient noise, Shapiro et al. (2005) cross-correlated one month of ambient noise data recorded on EarthScope US-Array stations across California. They measured short-period Rayleigh wave group speeds for hundreds of inter-receiver paths and used them to construct tomographic maps of California. The maps agreed very well with the known geology of the region, for example low velocity anomalies are co-located with sedimentary basins such as the San Joaquin Basin, and high velocity anomalies are associated with the igneous mountain ranges such as the Sierra Nevada. Almost simultaneously, Sabra et al. (2005b) produced interferometric surface waves by cross-correlating 18 days of ambient noise recorded on 148 stations in southern California. The tomographic maps they produced agree well with the known geology and previous seismic studies in the region. Since then, surface wave tomography using interferometric Rayleigh and Love waves, commonly referred to as ambient noise tomography, has become an increasingly employed method to successfully produce subsurface velocity models on regional and continental scales in areas such as the United States (Bensen et al.,

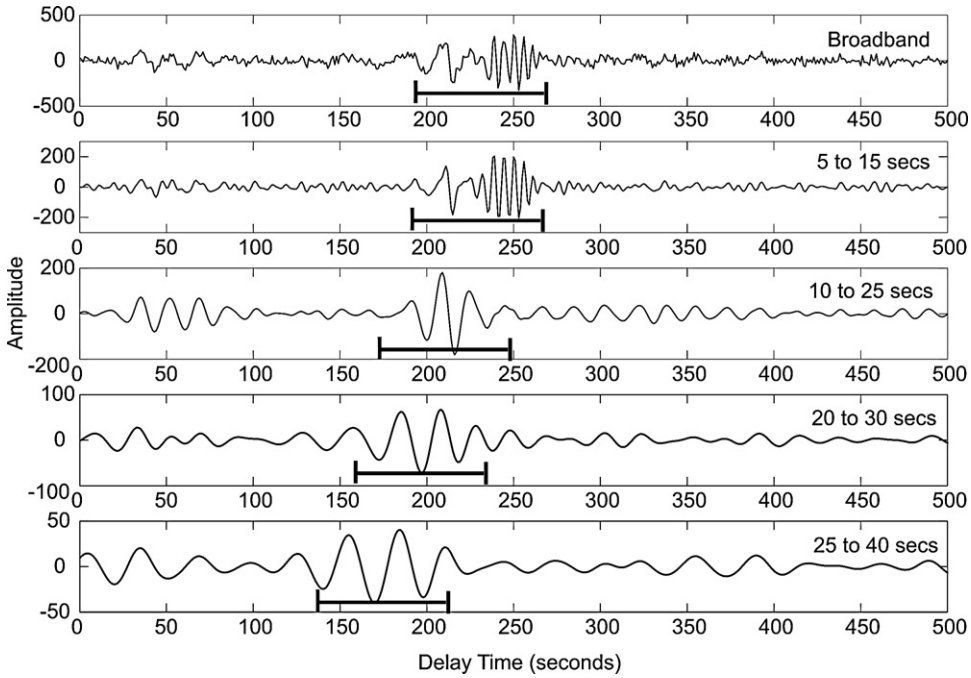

Fig. 4. Cross-correlation of approximately 6 months of noise data between JSA (Jersey) and KESW (Keswick, Lake District), with a path length of approximately 600 km. The raw, broad-band cross-correlation is shown at the top and progressively longer-period band-passes are given below. Horizontal bars show the approximate location of the dominant surface wave energy in each case. Note that the longer period waves arrive earlier than the shorter period waves.

2008; Lin et al., 2008; Shapiro et al., 2005; Sabra et al., 2005b; Liang and Langston, 2008), Australia (Arroucau et al., 2010; Rawlinson et al., 2008; Saygin and Kennett, 2010), New Zealand (Lin et al., 2007; Behr et al., 2010), Antarctica (Pyle et al., 2010), Iceland (Gudmundsson et al., 2007), China (Zheng et al., 2008; Li et al., 2009; Zheng et al., 2010), South Africa (Yang et al., 2008), Europe (Villaseñor et al., 2007; Yang et al., 2006), South Korea (Cho et al., 2007) the Tibetan Plateau (Yao et al., 2006, 2008; Li et al., 2009), and in this paper, Scotland.

Since seismic interferometry does not depend on the location of impulsive sources such as earthquakes, rather only the location of the receivers (which is usually under our control), the resolution of ambient noise tomography in relatively aseismic regions can be greater than that achieved by local surface wave tomography using earthquakes. The British Isles do experience earthquakes but these tend to be fairly small and infrequent (Baptie, 2010). This limits our ability to perform detailed local earthquake surface wave tomography. Teleseismic earthquakes are recorded on seismometers in the British Isles, however the short period surface waves that are required to image the upper crust tend to be attenuated over the long distances the waves must travel before being recorded. In addition, there is normally some error in the source location of earthquakes, whereas using interferometry we know precisely the locations of our "virtual" earthquakes since we choose where to place the seismometers. Background seismic noise tends to be dominated by the primary and secondary oceanic microseisms (around 12–14 s and 6–8 s period, respectively). Other sources of ambient seismic noise include micro-seismic events, wind and anthropogenic noise. Taking into account these aspects of the seismic interferometry method, the characteristics of ambient seismic noise and the limitations on traditional tomography methods in the region, it follows that the British Isles are ideally situated to apply ambient noise tomography.

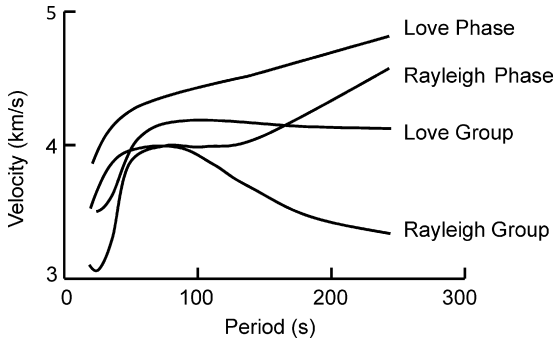

Fig. 5. Surface group and phase velocity dispersion curves for typical continental crust. From Fowler (2005) after Knopoff and Chang (1977). The group velocity is the speed at which the whole group or packet of waves making up the surface wave propagates whereas the phase velocity is the speed at which the phase of one particular frequency within the surface wave travels.

4. Ambient noise tomography in the Scottish Highlands

We applied ambient noise tomography to image the subsurface of the Scottish Highlands. The Reflections Under the Scottish Highlands (RUSH-II) network used in this study was a temporary deployment of twenty-four broadband seismometers. Initially deployed in the summer of 2001 in the shape of approximately three linear profiles with a station separation of approximately 15 km, the array forms a 2D array crossing the Great Glen Fault in the Scottish Highlands (Fig. 6). The main aims of the deployment were to determine the regional extent of major mantle reflectors beneath Scotland and to examine the relationship between any identified upper mantle reflectors and known Palaeozoic lithospheric-scale structures (Asencio et al., 2003). All twenty-four stations were installed by August 2001 and data was recorded almost continuously (except for a gap of approximately 6 months in 2002) for two-years. Bastow et al. (2007) describe the characteristics of the RUSH-II network in greater detail. A particularly interesting point to note from the Bastow et al. (2007) study was that they had to employ novel stacking techniques to suppress micro-seismic noise that contaminated

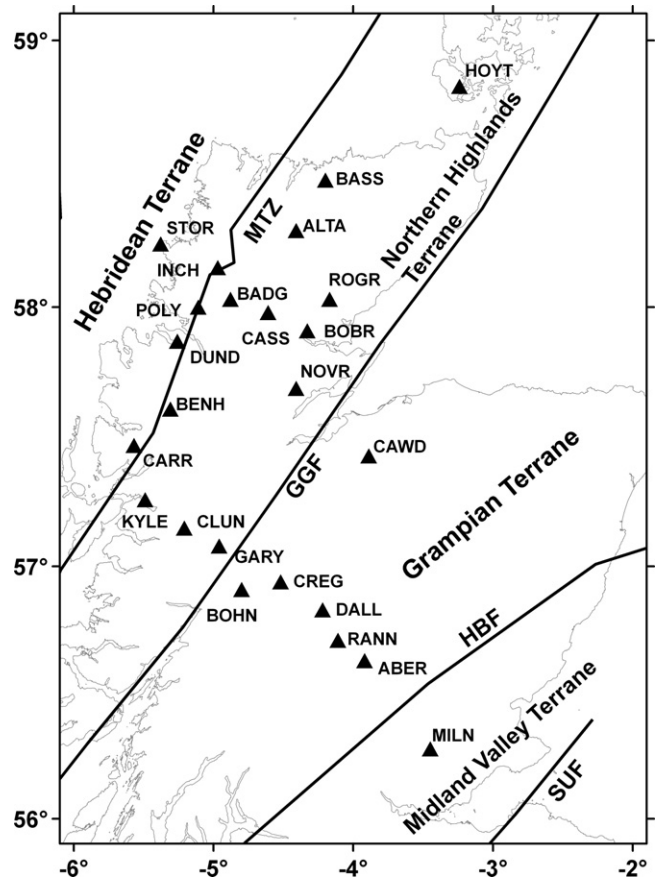

Fig. 6. Station location map for RUSH II array across the Scottish Highlands. Solid black lines represent the major tectonic and structural boundaries. SUF – Southern Uplands fault; HBF – Highland Boundary fault; GGF – Great Glen fault; MTZ – Moine Thrust Zone. From Woodcock and Strachan (2000).

the desired tele-seismic shear wave data. The abundance of ocean derived micro-seismic noise was such a problem because it lay in almost the same frequency range as the tele-seismic shear waves. Therefore the strong micro-seismic noise that propagates across Scotland creates a significant limitation for tele-seismic studies but a considerable opportunity for ANT.

4.1. Geology of the Scottish Highlands

For such a small country, the geology of Scotland is incredibly complex. The region is composed of a complicated amalgamation of several terranes (Bluck et al., 1992), from the Archaean Hebridean terrane north west of the Moine Thrust fault to the Silurian and Ordovician rocks of the Southern Uplands terrane, immediately north of the Iapetus Suture. The region has suffered a turbulent tectonic past and evidence of geological events from every period since the Precambrian can be found imprinted on its ~30 km thickness of rock. Fig. 6 shows a schematic summary of the main terranes of Scotland, separated by the major regional unconformities. A thorough description of the geological structure of the Scottish Highlands is given by Trewin (2002), however we provide a brief summary here.

The remote Hebridean Terrane is bounded to the north by the Outer Hebrides Fault and to the south by the Moine Thrust Zone. This terrane is composed of three principle rock units: (i) the Archaean to Palaeoproterozoic Lewisian Gneisses, overlain unconformably by (ii) Neoproterozoic, fluvial Torridonian sandstones which are in turn overlain by (iii) Cambrian to Ordovician clastic and carbonate marine shelf deposits. The Lewisian basement complex is formed from a variety of gneissose rocks with a very complex history that outcrop extensively on the Outer and Inner Hebrides and along the far north-west coast of the Scottish mainland. The thick (up to 6 km) Torridonian Sandstones were deposited in continental rift valleys or on the forelands of Rodinia, before the opening of the Iapetus Ocean. They outcrop widely in the north-west Scottish mainland and on the islands of Skye, Raasay and Rhum. Additionally, the Torridonian Sandstone subcrop extends as far as the Minch Fault to the west and the Great Glen Fault, 125 km to the southwest of Rhum. The Cambro-Ordovician shelf deposits are approximately 1 km thick and were deposited on a marine shelf on the passive margin of Laurentia. They lie unconformably on the Torridonian and Lewisian and extend over a distance of approximately 250 km, from the north coast of Scotland to Skye. The Moine Thrust Zone marks the north-west extent of the Caledonides on the British Isles, such that it separates the relatively undeformed foreland of the Hebridean Terrane from the extensively deformed, orogenic hinterland across the rest of the Scotland Highlands. Displacement along the Moine Thrust occurred as a result of NW-SE compression during the Caledonian orogeny (the most significant orogenic event to have affected the British Isles which resulted in the collision of Laurentia, Baltica and Avalonia and the closure of the Iapetus Ocean).

The geology of the Northern Highlands Terrane, bounded by the Moine Thrust to the North and the Great Glen Fault to the south, is dominated by the Caledonian mid to high-grade meta-sedimentary sequences of the Moine supergroup. The supergroup sediments were deposited as sands, silts and muds in a shallow marine environment on the margin of Laurentia and were metamorphosed as a result of the Caledonian orogeny. This event caused tens of kilometres of movement on the Moine Thrust Zone resulting in multiple phases of extensive recumbent folding of the Moine Supergroup. Gneissose inliers outcrop extensively across the Northern Terrane and are thought to represent uplifted sections of the basement complex on which the Moine Supergroup sediments were deposited. Geochemical, lithological and zircon dating studies have concluded that the inliers show similarities to the Lewisian gneisses (Woodcock and Strachan, 2000) and are therefore likely to have similar seismic characteristics. Dextral movement along the Great Glen Fault during the Carboniferous shifted the Northern Highland terrane northwards with respect to the Grampian Terrane. Therefore it may be reasonable to expect a difference in velocity structure across the Great Glen Fault.

The Grampian terrane, bounded by the Great Glen Fault to the north, is dominated geologically by the Dalradian Supergroup. The Dalradian sediments were deposited between ~800 and ~470Ma, consisting of a wide variety of facies such as rift basin sediments, deep marine turbidites, shallow marine sediments, tidal quartzites and glacial boulder beds. Dalradian sedimentation is thought to have resulted in a total deposited thickness of ~25 km. The Grampian terrane was widely metamorphosed during the Caledonian orogeny, where the Dalradian was tightly folded and sheared along predominantly NE-SW striking structures. Following this, younger granites, such as the Cairngorms and Glencoe, were intruded into the Northern and Grampian Highlands, their magmas likely to have originated from a subduction zone plunging northwards beneath Laurentia. It is likely that these large igneous centres have different seismic properties to the surrounding rock and therefore may be observable features of a detailed tomographic study across Scotland. Devonian sediments can be found along the Moray Firth coast and were deposited within the Orcadian Basin, the source material eroded from the surrounding Caledonian Mountains. These sediments are expected to appear as a low velocity anomaly located within seismically faster metamorphic rocks.

The Highland Boundary Fault marks the southern boundary of the metamorphic Caledonides of the Scottish Highlands and the northern limit of the Midland Valley terrane. This terrane is dominated by sediments of Devonian and Carboniferous age, such as the Old and New Red Sandstones and Carboniferous basin limestones. Previous geophysical studies, for example the Midland Valley Investigation by Seismology (three seismic refraction profiles across upper Palaeozoic basins in the Midland Valley), suggest that approximately 4–8 km of sediment overlies high velocity basement rock in the Midland Valley (Dentith and Hall, 1989, 1990). During the Carboniferous intense, intra-plate volcanism, associated with crustal reorganisation and thinning due to the Variscan orogeny in the south of England, affected the Midland Valley.

The Southern Uplands terrane lies between the Southern Upland Fault and the Iapetus Suture, a line representing the closure of the Iapetus Ocean due to the collision of Laurentia and Avalonia during the Caledonian orogeny. This terrane is dominated by an imbricate thrust zone of Ordovician and Silurian graywackes and shales, thought to originate as an accretionary prism that formed on the Laurentian margin above the northward plunging subduction zone that closed the Iapetus Ocean. The Southern Upland terrane is outside of our area of interest in this study.

4.2. Seismic interferometry across the Scottish Highlands

We have applied the ambient noise tomography method to noise data recorded on all 24 RUSH-II broadband seismometers. We mostly follow the data processing procedure as described in detail by Bensen et al. (2007) which is summarised as follows: first, we cut the continuous noise data into files of 24 h in length, then remove each seismometer's instrumental response, and the mean and linear trends from the day-files. To reduce the amount of storage space and computational time required, the data are then decimated to one sample per second. The next step involves applying time domain normalisation in order to remove the influence of large amplitude events such as earthquakes and other non-stationary noise sources from the subsequent cross-correlation. Bensen et al. (2007) describe various methods of applying time domain normalisation, however we decided that computationally less expensive one-bit normalisation (i.e. only the sign of the signal is retained) was satisfactory for our purposes since the British Isles are more or less aseismic. Finally, the single station day-files are spectrally whitened in order to create more broadband ambient noise records, and to reduce the effect of any monochromatic noise sources inherent in the data.

Cross-correlations are computed for each day between as many station pairs as possible, and the results are then stacked over the total time period available for each pair. Cross-correlations between stations with a separation of less than 50 km are rejected since those between stations that are separated by smaller distances do not produce useful results. Fig. 7 shows typical cross-correlations across the Scottish Highlands. The positive and negative lag times represent energy travelling in opposite directions between the pair of stations. Note that the cross-correlation functions can be asymmetric around zero delay time. This occurs when the ambient noise travels predominantly in one direction between the stations, and is a common characteristic of British interferometry due to the proximity of the Atlantic Ocean to the West, which is the dominant noise source. For example in Fig. 7b the arriving energy is predominantly on the positive (or causal) part of the cross-correlation, indicating that the ambient noise travelled dominantly in a direction from station STOR towards CAWD, so generally from West to East. Conversely in Fig. 7c the arriving energy is predominantly on the negative (acausal) component therefore the seismic noise travelled dominantly from KYLE towards RANN. Since asymmetry of the cross-correlations is prevalent in the British data and it is not always clear whether the causal or acausal component is better, we use the symmetric-component of the cross-correlation (i.e. the average of its causal and acausal parts) as our estimate of each inter-station seismogram.

A basic property of Rayleigh and Love waves is that they propagate as a series of different fundamental and higher modes, which are related to solutions of their governing wave equations (Aki and Richards, 2002). We concentrate our efforts on the fundamental modes since they are normally the most easily identified modes in interferometrically constructed surface waves. Once cross-correlations have been computed for a station pair and stacked over time giving an inter-receiver seismogram, a group velocity dispersion curve is estimated for the fundamental mode of the resulting virtual surface wave. A dispersion curve is a plot of

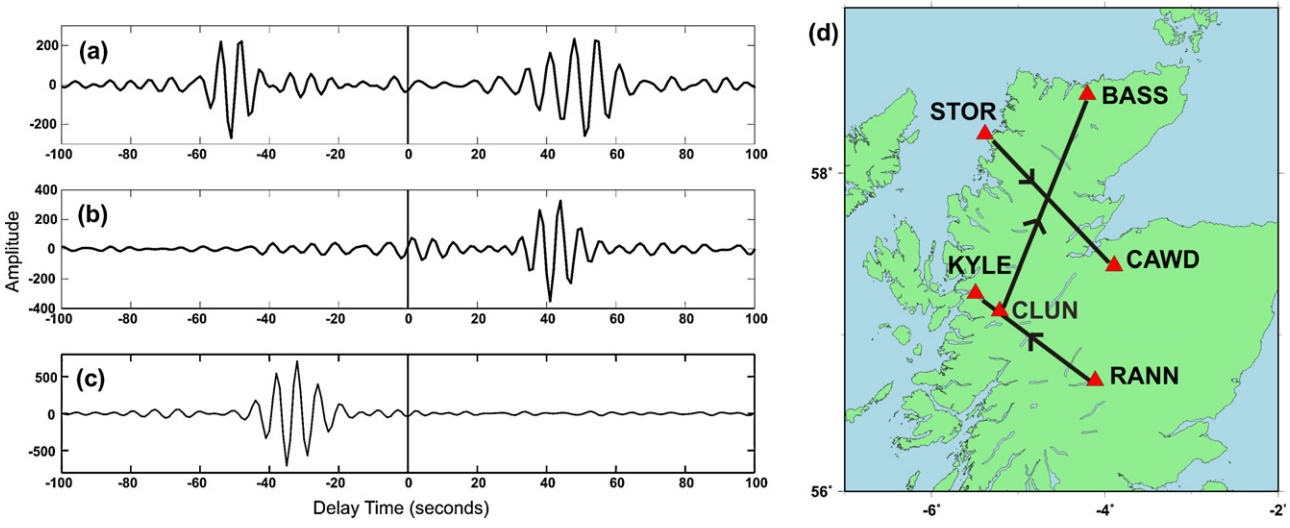

Fig. 7. Typical cross-correlations across the Scottish Highlands from ambient noise recordings. (a) Time-symmetric cross-correlation between CLUN and BASS; (b) one-sided, dominantly causal cross-correlation between STOR and CAWD; (c) one-sided, dominantly acausal cross-correlation between RANN and KYLE. Waveforms are band-passed between 5 and 10 s period. The positive and negative parts of the waveforms represent energy travelling in opposite directions between two receivers. (d) Location map showing seismic stations (triangles) and direction of travel between the virtual source and receiver (black arrows).

the speed of travel of a surface wave versus period which describes the dispersion of each component period in the surface wave, similar to those in Fig. 5. We do this by applying the multiple phase-matched filter method of Herrmann (2005). Here, the fundamental mode is isolated from other unwanted arrivals such as those due to higher mode surface waves or high frequency noise using a standard time-frequency filter. Its dispersion properties can then be computed and group velocities for all possible periods, in this case between 5 and 30 s approximately, are picked interactively on a computer.

If the method of ambient noise surface wave estimation is robust, it should be repeatable in time. Therefore, four more estimates of every possible surface wave fundamental mode dispersion curve were picked, where each is constructed by stacking correlations from an equal number of randomly-selected days of noise, and where each individual day can appear in only one random stack. Thus, in total we obtain five completely independent group velocity estimates for each period. The standard deviation of these curves provides an estimate of the uncertainty in the average velocity measurement at each period.

While the output measurement from the multiple phase-matched filter step described above is the average group velocity along a raypath, what is actually measured during the above process is the peak arrival time of the wave packet at each individual frequency. Hence, the quantity measured is the average travel-time and its standard deviation. These inter-receiver travel-time uncertainties are used to weight the relative importance of their associated paths in the tomographic inversion.

4.3. Rayleigh wave ambient noise tomography

The aim of the tomography step is to estimate the seismic surface wave velocity at different periods across the northwest Scottish Highlands, given the dataset described above which defines only the average velocity between station pairs. Since the travel-time measurements occur along multiple paths, we use an iterative, non-linear inversion method which makes small adjustments to a homogeneous velocity starting model, recalculating the travel-times through this model at each iteration, until the differences between calculated and observed travel-times are

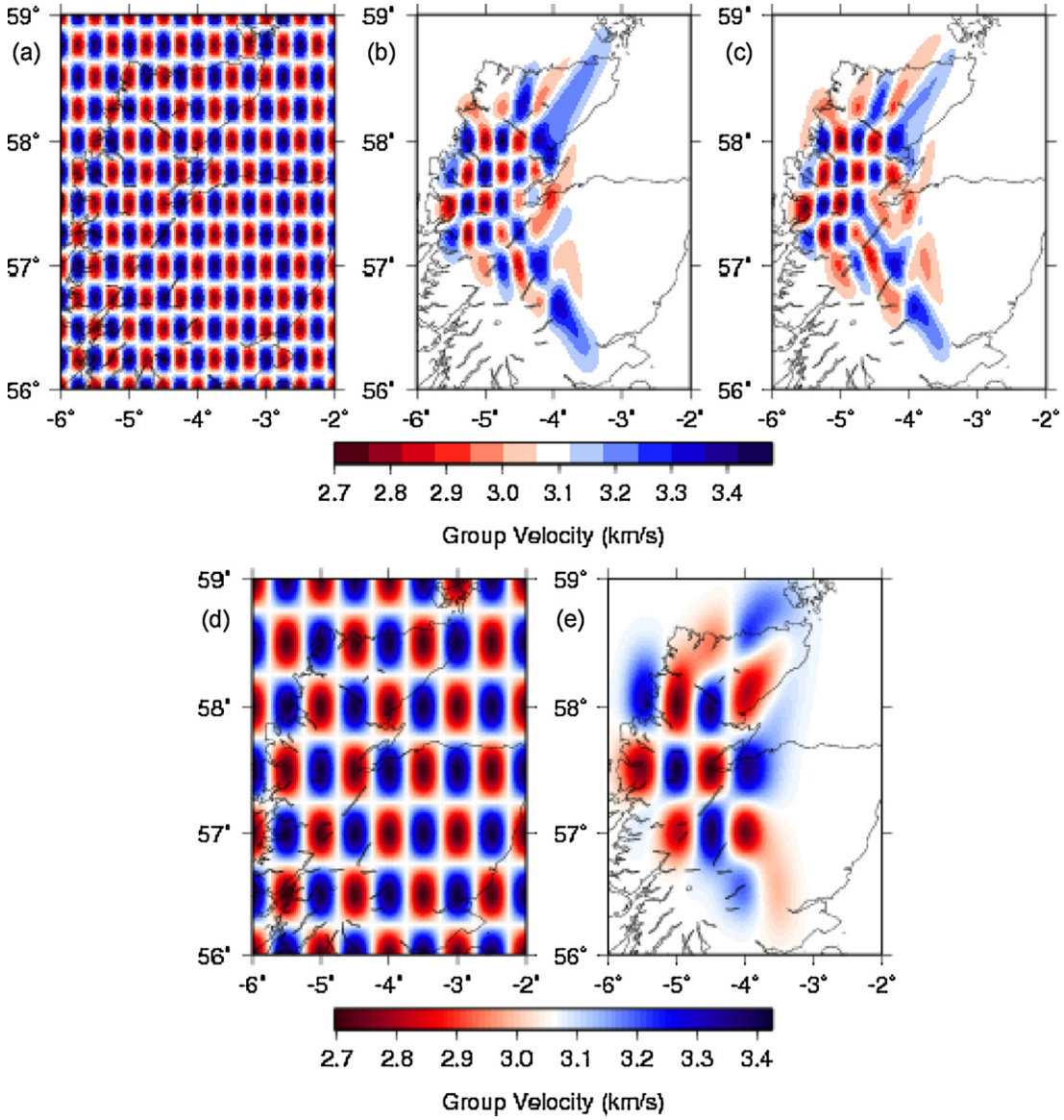

Fig. 8. Results of chequerboard resolution test. (a) Synthetic chequerboard model, cell size ~25 km; (b) recovered solution model using 5 s raypaths; (c) recovered solution model using 12 s raypaths; (d) synthetic chequerboard model, cell size ~50 km; (e) recovered solution model using 20 s raypaths.

acceptably small, subject to regularisation constraints which aim to avoid geologically unrealistic models (Rawlinson and Sambridge, 2005). We use the FMST tomography package developed by Nick Rawlinson at the Australian National University to perform our Rayleigh wave tomography.

Before a tomographic inversion is performed with real surface wave travel time data, it is important to test how well the geometry of stations and virtual sources might resolve the subsurface structure. This is done by generating known, synthetic velocity models to represent the Earth's subsurface, computing synthetic data for each model, performing tomography on the synthetic data and testing how well the resulting velocity model estimates match the original synthetic Earth models. The method we apply here to test the resolution of our problem is the so-called chequerboard test (e.g. Iyer and Hirahara, 1993). Synthetic inter-station travel-times are calculated using the same station geometry as for the real data, but through a velocity model consisting of a grid of alternating faster and slower velocity cells resembling a chequer board (Fig. 8a). Uncertainties, in the form of Gaussian noise, are assigned to the synthetic travel times which are then treated as the "observed" travel-times to determine the resolving power of the given geometry. Fig. 8 shows the result of a synthetic chequerboard resolution test for the RUSH II stations in Fig. 6.

Fig. 8a shows a chequerboard model where the cells are approximately 25 by 25 km in size and Fig. 8b and c shows the recovered solution models for 5 and 12 s period, respectively. Fig. 8d shows a chequerboard model where the cells are approximately 50 by 50 km in size and Fig. 8e shows the recovered solution model for 20 s period. Only ray-paths for which a real travel-time measurement at the specified period exists have their equivalent synthetic travel-time included in the appropriate inversions. Therefore these tests are expected to give a reasonably realistic idea of the resolving power of the real data at each period. Since the data here are calculated between stations, there is no data coverage outside of the area enclosed by the seismometer array, therefore the chequerboard pattern is not resolved there as expected. For the 5 and 12 s tests, the resolution in the area enclosed by the array is excellent, and we conclude that the data coverage here is sufficient to resolve features down to roughly 25 km length-scale and above. For the 20 s test, resolution within the area enclosed by the array is still reasonable, but the smallest chequerboard size that can be recovered well at this period has around 50 km length-scale. This is because the number of well-constrained travel-time measurements decreases with increasing period, hence the ray-path coverage has been significantly depleted by 20 s (Fig. 9). Note also that some smearing of the chequerboard pattern occurs towards the edges of the resolvable area. Note, however, that the examples given in Fig. 8 are for a best-case-scenario where minimal regularisation is applied. Errors and uncertainties in the real data may require more severe regularisation and hence degrade the resolution further.

Using a 2-D tomography scheme similar to that applied by Rawlinson and Sambridge (2005), Rawlinson et al. (2006) and Rawlinson and Urvoy (2006) as described above, we inverted travel-time datasets for 5, 12 and 20 s period. We chose to use a 7.5 by 7.5 km grid for the inversions since this is much smaller than the minimum length-scale that is resolvable by the data, therefore it will minimise any leakage of true Earth structures at lengthscales smaller than the resolveable feature size (approximately >25 km) into our maps (Trampert and Sneider, 1996). The starting models were homogeneous, which is not an uncommon practise in seismic tomography, where the velocities were chosen to be the average measured for that period. However, it is worth noting that as with any particular starting model, using a homogeneous model can potentially bias the solution since the solution might represent a locally-best rather than a globally optimal data fit within the model space. Tomographic maps were produced for many different combinations of regularisation parameters and the weighted root mean square of the data residuals was calculated for each map such that

$$RMS_W = \sqrt{\frac{1}{N}\sum_{i=1}^{N}\frac{x_i^2}{\sigma_i^2}} \quad (1)$$

where N is the number of ray-paths, and x_i and σ_i are the travel-time residual and uncertainty associated with a raypath i. The result is a dimensionless number that provides a measure of the normalised misfit of the computed data post-inversion through the

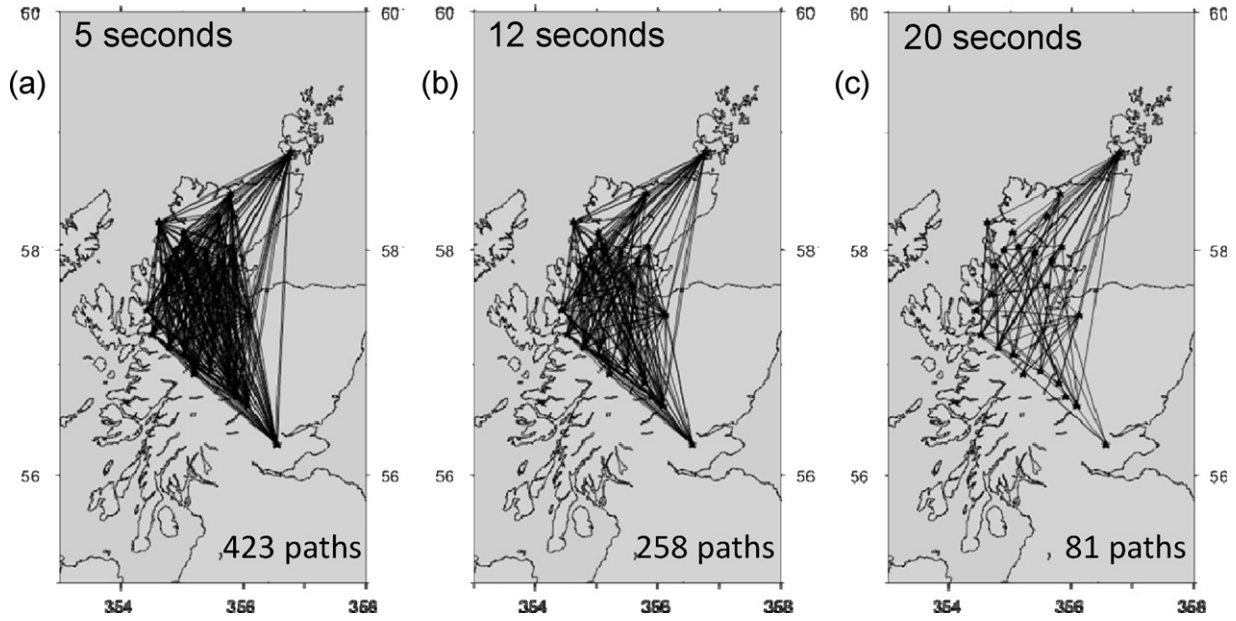

Fig. 9. Ray-paths (black lines) for (a) 5 s, (b) 12 s and (c) 20 s period.

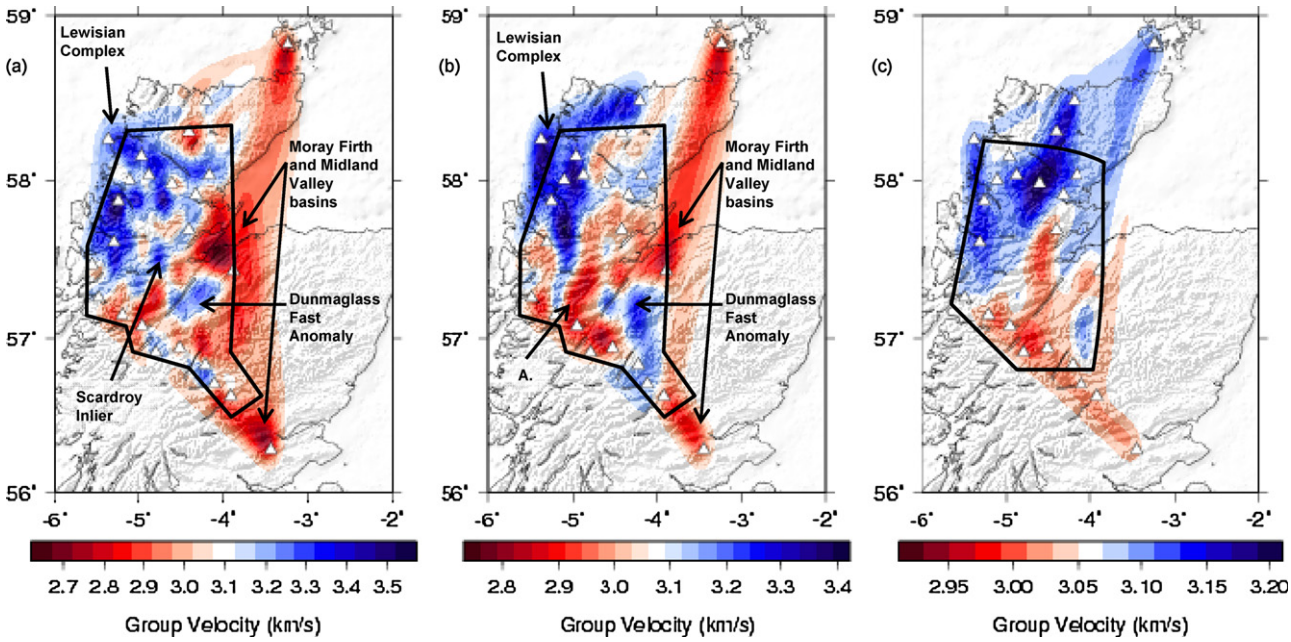

Fig. 10. Rayleigh wave group velocity maps of the Scottish Highlands from cross-correlations of ambient seismic noise between RUSH-II stations (white triangles) for (a) 5 s; (b) 12 s and (c) 20 s period. Areas with reasonable resolution are approximately located within the black polygons.

estimated Earth model, for which the *a priori* uncertainty of the data is taken into account. As an approximate guide, if the value of RMS_W is significantly greater than 1 then the data fit is potentially significantly affected by the influence of the choice of regularisation parameters. However if the value of RMS_W is <1 then the solution model fits the observed data to within data uncertainties. In order to allow for statistical uncertainty or variation in RMS_W we choose our upper limit for RMS_W to be 1.3. Initial inversions that were found to have high RMS_W values have their highest residual paths removed sequentially from subsequent inversions until their RMS_W value falls below the acceptable threshold. The main features of the computed maps are all robust to this removal step, but this step is nevertheless advantageous as it ensures that particularly anomalous data (which are likely due to some undetected error in the semi-automated processing sequence) do not affect the final results. The resulting Rayleigh wave group velocity maps are shown in Fig. 10. For comparison, Fig. 11 shows surface geology, gravity and aeromagnetic maps of Scotland.

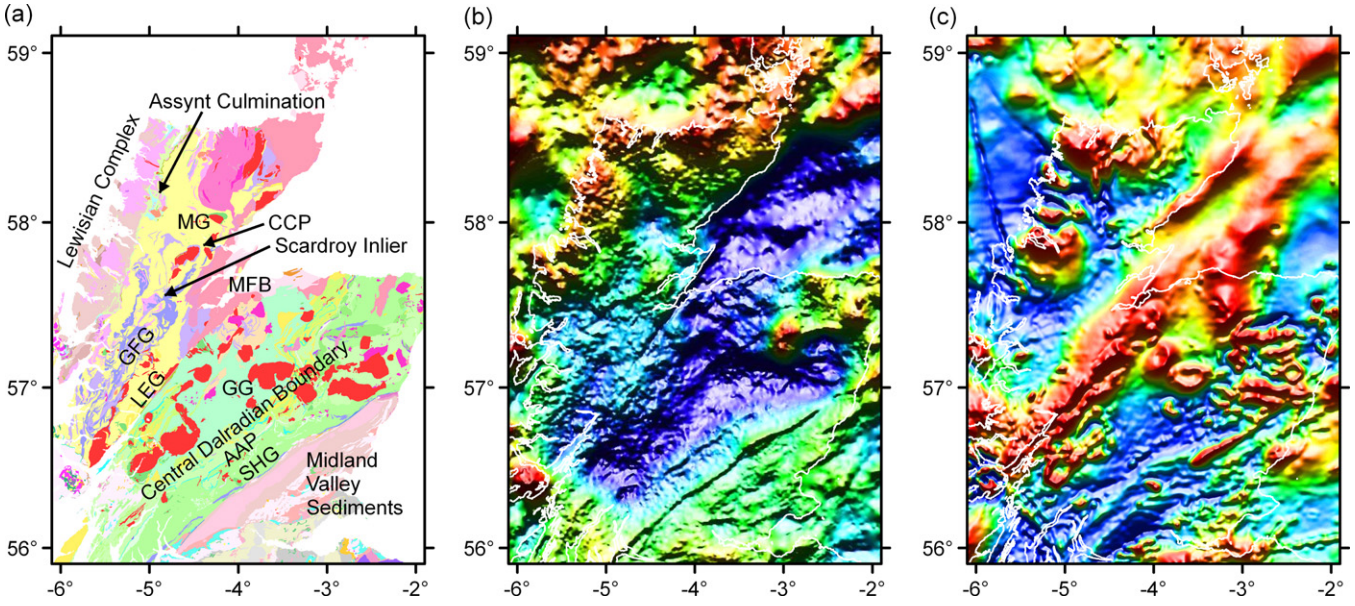

Fig. 11. Surface geology and geophysical potential field maps of Scotland. (a) 1:625000 surface geology map of Scotland. Different groups within the Moine and Dalradian supergroups are denoted as follows: MG – Morar Group; GFG – Glenfinnan Group; LEG – Loch Eil Group; GG – Grampian Group; AAG – Argyll and Appin Group; SHG – Southern Highlands Group. MFB –Moray Firth Basin. CCP – Carn Chuinneag Pluton. (b) Shaded relief gravity anomaly map. Red colours indicate positive anomalies and blue colours indicate negative anomalies. (c) Shaded relief aeromagnetic anomaly map. Red colours indicate positive anomalies and blue colours indicate negative anomalies. Reproduced with permission from the British Geological Survey.

5. Discussion

A number of interesting geological features can be identified on the Rayleigh wave maps in Fig. 10, although they do not all obviously match to the terrane structure of Scotland and geology and geophysical maps in Fig. 11. Overall, shallow sediments are shown as low velocities and in contrast higher velocities often characterise igneous and metamorphic rocks. In addition, there is a general increase in velocity from south-east to north-west across the Scottish Highlands at all periods.

For the 5 s map, which is sensitive to the shallow upper crust above approximately 8 km depth, low velocity anomalies may be identified in the Midland Valley and Moray Firth sedimentary basins, however it is worth noting that these anomalies occur at the very edges of the area with acceptable resolution. A transition from low to high velocity is observable in the southern highlands, co-located with the Central Dalradian Boundary (Fig. 11c). A similar transition from higher to lower values can also be observed in this area on the gravity anomaly map of Scotland (Fig. 11b). Trewin (2002) suggests that there is geological and geophysical evidence for the continuation of the Midland Valley northwards beyond the Highland Boundary Fault, with the true crustal terrane boundary hidden by the Dalradian in the Southern Highlands. Our results also suggest that the true crustal boundary at depth between the Midland Valley and Grampian terranes is located approximately 35 km to the north west of the Highland Boundary Fault.

The low velocity anomaly in the Moray Firth basin extends towards the south west and northwards along the north east coast. This feature correlates with a strong positive anomaly on the aeromagnetic map in Fig. 11a. The low velocities close to the coast can likely be attributed to the thick, sedimentary pull-apart basin in the Moray Firth and to the Devonian sediments situated along the north east coast.

A relatively fast anomaly in the region of Dunmaglass, centred at approximately (−4.4°E, 57.2°N) southeast of the Great Glen Fault, cannot easily be correlated with features of the surface geology, magnetic or gravity maps. Although its origin is unclear, comparisons with the locations of major faults across Scotland show that the southern and northern margins of the Dunmaglass anomaly appear to be approximately bounded by faults. A strong low velocity anomaly north of the Great Glen Fault correlates reasonably well with the Loch Eil group of the Moine supergroup (Fig. 11c).

Fast velocity anomalies in the very north west of mainland Scotland are coincident with the old Lewisian rock of the Hebridean terrane and can also be associated with gravity and magnetic anomalies. A slight bulge in the east of the fast velocity anomaly here may be attributed to the Assynt culmination, which can be identified on the surface geology and gravity maps in Fig. 11. Immediately to the south-east of the Assynt culmination a low velocity anomaly is co-located with the Lairg gravity low (Leslie et al., 2010), located on the gravity map in Fig. 11b at approximately (−4.5°E, 58.0°N). One result of movement on thrust faults, such as the Sgurr Beag thrust, throughout the Northern Highlands terrane is that in some areas Lewisian rocks have been uplifted nearer to the surface. Small, high velocity anomalies in the Northern Highlands terrane may be due to some of these features (which may or may not be observable in the surface Geology). For example the isolated fast velocity feature at (−4.7°E, 57.5°N) is approximately co-located with the Scardroy inlier, a known Lewisian inlier in central Ross-shire. Overall, the 5 s map shows a gradual increase in seismic velocity from south-east to north-west across Scotland.

The 12 s map is sensitive to seismic velocity anomalies down to the mid-crust at around 15 km depth. Low velocity anomalies again coincide with the Midland Valley and the Moray Firth basin. The low velocity region that was observed north of the Great Glen at 5 s period can be seen to extend northwards into the Northern Highlands terrane (Fig. 10b – A.) and appears to track along the Glenfinnan group, where most of the Lewisian inliers within the Northern terrane are located, terminating immediately north east of the Carn Chuinneag pluton (Fig. 11c). The western part of the Dunmaglass anomaly is still present at 12 s, however the eastern part appears to have moved and now extends towards the south east. The high velocity anomaly ascribed to the Lewisian complex in the far northwest at 5 s is also present at 12 s.

The 20 s map is sensitive down to a depth of approximately 30 km. Although this map is certainly of lower resolution than those at 5 s and 12 s, a general increase in velocity from south to north can be observed. 30 km depth is consistent with the average crustal thickness in the Scottish Highlands. Therefore the velocity structure here can be explained by a shallowing of the Moho northwards across the region, since the 20 s period surface waves are sensitive to more and more high velocity mantle material towards the north. Interpreted depths of the Moho across Scotland range from 36 km in the Midland Valley to 22 km off Cape Wrath (Trewin, 2002), and this is also consistent with the results of the LISPB experiments in Scotland (e.g. Bamford et al., 1978; Barton, 1992). The sharp increase in crustal thickness observed by Di Leo et al. (2009) west of the Moine thrust is not observed in our results.

6. Conclusions

In this paper we have described the background of seismic interferometry and the ambient noise tomography method. We have shown that seismic interferometry can be used to compute inter-receiver surface waves using ambient noise data recorded in the British Isles and specifically in detail across the Scottish Highlands. This greatly increases the number of potential ray-paths along which seismic data are available within the British Isles compared with traditional earthquake and explosive source methods. We have presented the first surface wave group velocity maps of the Scottish Highlands from ambient seismic noise and have shown that they contain useful information about the crust and upper mantle that is consistent with geological features of the region. Ambient noise studies in other parts of the world have inverted for 3-D variations in subsurface structure with depth, produced Love as well as Rayleigh wave tomographic maps, and measured phase velocities in addition to group velocities (Yao et al., 2006; Bensen et al., 2009; Lin et al., 2008 etc.). Rayleigh wave group speed maps produced for the British Isles from ambient noise so far are promising and we expect more exciting results in the near future. Further work will aim to use Love as well as Rayleigh waves and increase the number of stations used in order to increase the data coverage across the region.

Acknowledgements

The seismic data used in this study were obtained from the IRIS Data Management Centre. Thanks are extended to Godfrey Fitton, Roger Hipkin and Kathryn Goodenough for many helpful discussions, and to the reviewers whose feedback improved this manuscript. Many of the figures in this paper were prepared using GMT (Wessel and Smith, 1995).

References

Aki, K., Richards, P., 2002. Quantitative Seismology, 2nd ed. Ellis, University Science Books, Sausalito, CA.

Arroucau, P., Rawlinson, N., Sambridge, M., 2010. New insight into Cainozoic sedimentary basins and Palaeozoic suture zones in southeast Australia from ambient noise surface wave tomography. Geophysical Research Letters 37, L07303.

Asencio, E., Knapp, J., Owens, T., Helffrich, G., 2003. Mapping fine-scale heterogeneities within the continental mantle lithosphere beneath Scotland: combining active and passive source seismology. Geology 31, 447–480.

Bakulin, A., Calvert, R., 2006. The virtual source method: theory and case study. Geophysics 71, SI139–SI150.
Bamford, D., Nunn, K., Prodehl, C., Jacob, B., 1978. LISPB IV. Crustal structure of northern Britain. Geophysical Journal of the Royal Astronomical Society 54, 43–60.
Baptie, B., 2010. Seismogenesis and state of stress in the UK. Tectonophysics 482, 150–159.
Barton, P., 1992. LISPB revisited: a new look under the Caledonides of northern Britain. Geophysical Journal International 110, 371–391.
Bastow, I., Owens, T., Helffrich, G., Knapp, J., 2007. Spatial and temporal constraints on sources of seismic anisotropy: Evidence from the Scottish highlands. Geophysical Research Letters 34 (5), L05305.
Behr, Y., Townend, J., Bannister, S., Savage, M., 2010. Shear velocity structure of the Northland Peninsula, New Zealand, inferred from ambient noise correlations. Journal of Geophysical Research 115, B05309.
Bensen, G.D, Ritzwoller, M.H., Barmin, M.P., Levshin, A.L., Moschetti, M.P., Shapiro, N.M., Yang, Y., 2007. Processing seismic ambient noise data to obtain reliable broad-band surface wave dispersion measurements. Geophysical Journal International 169, 1239–1260.
Bensen, G.D., Ritzwoller, M.H., Shapiro, N.M., 2008. Broadband ambient noise surface wave tomography across the United States. Journal of Geophysical Research 113 (B5), 1–21.
Bensen, G.D., Ritzwoller, M.H., Yang, Y., 2009. A 3-D shear velocity model of the crust and uppermost mantle beneath the United States from ambient seismic noise. Geophysical Journal International 177 (3), 1177–1196.
Bluck, B., Gibbons, W., Ingham, J., 1992. Terranes. In: Cope, J.C., Ingham, J.K., Rawson, P.F. (Eds.), Atlas of Palaeogeography and Lithofacies, 13. Geological Society of London Memoirs, pp. 1–4.
Campillo, M., Paul, A., 2003. Long-range correlations in the diffuse seismic coda. Science 299, 547–549.
Cho, K., Herrmann, R., Ammon, C., Lee, K., 2007. Imaging the upper crust of the Korean peninsula by surface-wave tomography. Bulletin of the Seismological Society of America 97 (1B), 198–207.
Claerbout, J., 1968. Synthesis of a layered medium from its acoustic transmission response. Geophysics 33, 264–269.
Cole, S., 1988. Examination of a passive seismic dataset using beam steering. Stanford Exploration Project Report 57, 417–426.
Cole, S., 1995. Passive seismic and drill-bit experiments using 2-D arrays. Ph.D. thesis, Stanford University.
Curtis, A., Gerstoft, P., Sato, H., Snieder, R., Wapenaar, K., 2006. Seismic interferometry – turning noise into signal. The Leading Edge 25 (9), 1082–1092.
Curtis, A., Nicolson, H., Halliday, D., Trampert, J., Baptie, B., 2009. Virtual seismometers in the subsurface of the Earth from seismic interferometry. Nature Geoscience 2 (10), 700–704.
Curtis, A., Halliday, D., 2010a. Source–receiver wave field interferometry. Physical Review E 81, 046601.
Curtis, A., Halliday, D., 2010b. Directional balancing for seismic and general wavefield interferometry. Geophysics 75 (1), SA1–SA14.
Dentith, M., Hall, J., 1989. MAVIS: an upper crustal seismic refraction experiment in the Midland Valley of Scotland. Geophysical Journal International 99, 627–643.
Dentith, M., Hall, J., 1990. MAVIS: geophysical constraints on the structure of the Carboniferous basin of West Lothian, Scotland. Transactions of the Royal Society of Edinburgh 81, 117–126.
Derode, A., Larose, E., Campillo, M., Fink, M., 2003. How to estimate the Green's function of a heterogeneous medium between two passive sensors? Application to acoustic waves. Applied Physics Letters 83 (15), 3054–3056.
Di Leo, J., Bastow, I., Helffrich, G., 2009. Nature of the Moho beneath the Scottish Highlands from a receiver function perspective. Tectonophysics 479, 214–222.
Dong, S., He, R., Schuster, G., 2006. Interferometric prediction and least squares subtraction of surface waves. 76th Annual International Meeting. SEG (Expanded Abstracts) 2783–2786.
Draganov, D., Wapenaar, K., Thorbecke, J., 2006. Seismic interferometry: reconstructing the earth's reflection response. Geophysics 71, SI61–SI70.
Duvall, T., Jefferies, S.M., Harvey, J.W., Pomerantz, M.A., 1993. Time–distance helioseismology. Nature 362, 430–432.
Dziewonski, A., Bloch, S., Landisman, M., 1969. A technique for analysis of transient seismic signals. Bulletin of the Seismological Society of America 59, 427–444.
Dziewonski, A., Mills, J., Bloch, S., 1972. Residual dispersion measurement—a new method of surface-wave analysis. Bulletin of the Seismological Society of America 62, 129–139.
Fowler, C., 2005. The Solid Earth: An Introduction to Global Geophysics, 2nd ed. Cambridge University Press.
Gudmundsson, Ó., Khan, A., Voss, P., 2007. Rayleigh-wave group-velocity of the Icelandic crust from correlation of ambient seismic noise. Geophysical Research Letters 34, L14314.
Halliday, D., Curtis, A., van-Manen, D.-J., Robertsson, J., 2007. Interferometric surface wave isolation and removal. Geophysics 72 (5), A69–A73.
Halliday, D., Curtis, A., 2008. Seismic interferometry, surface waves and source distribution. Geophysical Journal International 175 (3), 1067–1087.
Halliday, D., Curtis, A., Kragh, E., 2008. Seismic surface waves in a suburban environment – active and passive interferometric methods. The Leading Edge 27 (2), 210–218.
Halliday, D., Curtis, A., 2009. Seismic interferometry of scattered surface waves in attenuative media. Geophysical Journal International 178 (1), 419–446.
Halliday, D., Curtis, A., Vermeer, P., Strobbia, C., Glushchenko, A., van-Manen, D.-J., Robertsson, J., 2010. Interferometric ground-roll removal: attenuation of direct and scattered surface waves in single-sensor data. Geophysics 75 (2), SA15–SA25.
Herrmann, R., 2005. Surface waves, receiver functions and crustal structure. Computer Programs for Seismology v.3.30, St.Louis University.
Iyer, H., Hirahara, K., 1993. Seismic Tomography: Theory and Practise. Chapman and Hall, London.
King, S., Curtis, A., Poole, T., 2010. Interferometric velocity analysis using physical and non-physical energy. Geophysics 76 (1), 35–49.
Knopoff, L., Chang, F., 1977. The inversion of surface wave dispersion data with random errors. Journal of Geophysics 43, 299–310.
Larose, E., Derode, A., Clorennec, D., Margerin, L., Campillo, M., 2005. Passive retrieval of Rayleigh waves in disordered elastic media. Physical Review E72 (4), 046607.
Leslie, G., Krabbendam, M., Kimbell, G., Strachan, R., 2010. Regional-scale lateral variation and linkage in ductile thrust architecture: the Oykel Transverse Zone, and mullions, in the Moine Nappe, NW Scotland. The Geological Society of London Special Publication 335, 359–381.
Li, H., Su, W., Wang, C.W., Huang, Z., 2009. Ambient noise Rayleigh wave tomography in western Sichuan and eastern Tibet. Earth and Planetary Science Letters 282, 201–211.
Liang, C., Langston, C., 2008. Ambient seismic noise tomography and structure of eastern North America. Journal of Geophysical Research 113.
Lin, F., Ritzwoller, M.H., Townend, J., Bannister, S., Savage, M.K., 2007. Ambient noise Rayleigh wave tomography of New Zealand. Geophysical Journal International 170 (2), 649–666.
Lin, F., Moschetti, M.P., Ritzwoller, M.H., 2008. Surface wave tomography of the western United States from ambient seismic noise: Rayleigh and Love wave phase velocity maps. Geophysical Journal International 173 (1), 281–298.
Lobkis, O., Weaver, R., 2001. On the emergence of the Green's function in the correlations of a diffuse field. The Journal of the Acoustical Society of America 110 (6), 3011.
Lu, R., Willis, M., Campman, X., Ajo-Franklin, J., Toksoz, M.N., 2008. Redatuming through a salt canopy and target-oriented salt-flank imaging. Geophysics 73, S63–S71.
Pawlak, A., Eaton, D., Bastow, I., Kendall, J.-M., Helffrich, G., Wookey, J., Snyder, D., 2010. Crustal structure beneath Hudson Bay from ambient-noise tomography: Implications for basin formation. Geophysical Journal International 184 (1), 65–82.
Pyle, M., Wiens, D., Nyblade, A., Anandakrishnan, S., 2010. Crustal structure of the Transantarctic Mountains near the Ross Sea from ambient seismic noise tomography. Journal of Geophysical Research 115, B11310.
Rawlinson, N., Sambridge, M., 2005. The fast marching method: an effective tool for tomographic imaging and tracking multiple phases in complex layered media. Exploration Geophysics 36, 341–350.
Rawlinson, N., Reading, A., Kennett, B., 2006. Lithospheric structure of Tasmania from a novel form of teleseismic tomography. Journal of Geophysical Research 111, B02301.
Rawlinson, N., Urvoy, M., 2006. Simultaneous inversion of active and passive source datasets for 3-D seismic structure with application to Tasmania. Geophysical Research Letters 33 (24), 1–5.
Rawlinson, N., Sambridge, M., Saygin, E., 2008. A dynamic objective function technique for generating multiple solution models in seismic tomography. Geophysical Journal International 174, 295–308.
Rickett, J., Claerbout, J., 1999. Acoustic daylight imaging via spectral factorization: helioseismology and reservoir monitoring. The Leading Edge 18 (957).
Sabra, K., Gerstoft, P., Roux, P., Kuperman, W.A., Fehler, M.C., 2005a. Extracting time-domain Green's function estimates from ambient seismic noise. Geophysical Research Letters 32 (3), 1–5.
Sabra, K., Gerstoft, P., Roux, P., Kuperman, W.A., Fehler, M.C., 2005b. Surface wave tomography from microseisms in Southern California. Geophysical Research Letters 32, L14311.
Saygin, E., Kennett, B., 2010. Ambient seismic tomography of Australian continent. Tectonophysics 481, 116–125.
Shapiro, N., Campillo, M., 2004. Emergence of broadband Rayleigh waves from correlations of the ambient seismic noise. Geophysical Research Letters 31 (7), 1615–1619.
Shapiro, N., Campillo, M., Stehly, L., Ritzwoller, M.H., 2005. High-resolution surface-wave tomography from ambient seismic noise. Science 307, 1615.
Slob, E., Draganov, D., Wapenaar, K., 2007. Interferometric electromagnetic Green's functions representations using propagation invariants. Geophysical Journal International 169, 60–80.
Snieder, R., 2004. Extracting the Green's function from the correlation of coda waves: a derivation based on stationary phase. Physical Review E 69 046610.1-046610.8.
Trampert, J., Sneider, R., 1996. Model estimations biased by truncated expansions: possible artifacts in seismic tomography. Science 271, 1257–1260.
Trewin, N., 2002. Geology of Scotland, 4th ed. Geological Society Publishing House.
van-Manen, D., Robertsson, J., Curtis, A., 2005. Modeling of wave propagation in inhomogeneous media. Physical Review Letters 94, 164301–164304.
van-Manen, D., Curtis, A., Robertsson, J., 2006. Interferometric modeling of wave propagation in inhomogeneous elastic media using time reversal and reciprocity. Geophysics 71 (4), SI47–SI60.
van-Manen, D., Robertsson, J., Curtis, A., 2007. Exact wavefield simulation for finite-volume scattering problems. Journal of the Acoustical Society of America 122 (4), EL115–EL121.

Villaseñor, A., Yang, Y., Ritzwoller, M.H., Gallart, J., 2007. Ambient noise surface wave tomography of the Iberian Peninsula: Implications for shallow seismic structure. Geophysical Research Letters 34 (11), 1–5.
Wapenaar, K., 2003. Synthesis of an inhomogeneous medium from its acoustic transmission response. Geophysics 68 (5), 1756–1759.
Wapenaar, K., 2004. Retrieving the elastodynamic Green's function of an arbitrary homogeneous medium by cross correlation. Physical Review E 69, 046610.
Wapenaar, K., Fokkema, J., 2006. Green's function representations for seismic interferometry. Geophysics 71, S133–S144.
Wapenaar, K., Ruigrok, E., van der Neut, J., Draganov, D., 2011. Improved surface-wave retrieval from ambient seismic noise by multi-dimensional deconvolution. Geophysical Research Letters 38, L01313.
Weaver, R., Lobkis, O., 2001. Ultrasonics without a source: thermal fluctuation correlations at MHz frequencies. Physical Review Letters 87 (13), 134301.
Weaver, R., Lobkis, O., 2002. On the emergence of the Green's function in the correlations of a diffuse field: pulse-echo using thermal phonons. Ultrasonics 40 (1–8), 435–439.
Wessel, P., Smith, W., 1995. New version of the generic mapping tools released. Eos, Transactions, American Geophysical Union 72, 329.
Woodcock, N., Strachan, R., 2000. Geological History of Britain and Ireland. Blackwell Science.
Yang, Y., Ritzwoller, M.H., Levshin, A.L., Shapiro, N.M., 2006. Ambient noise Rayleigh wave tomography across Europe. Geophysical Journal International 168 (1), 259.
Yang, Y., Ritzwoller, M.H., 2008. Characteristics of ambient seismic noise as a source for surface wave tomography. Geochemistry Geophysics Geosystems 9 (2), Q02008.
Yang, Y., Li, A., Ritzwoller, M.H., 2008. Crustal and uppermost mantle structure in southern Africa revealed from ambient noise and teleseismic tomography. Geophysical Journal International 174 (1), 235–248.
Yao, H., van der Hilst, R., de Hoop, M., 2006. Surface-wave array tomography in SE Tibet from ambient seismic noise and two-station analysis – I. Phase velocity maps. Geophysical Journal International 166, 732–744.
Yao, H., Beghein, C., van der Hilst, R., 2008. Surface wave array tomography in SE Tibet from ambient seismic noise and two-station analysis – II. Crustal and upper-mantle structure. Geophysical Journal International 173, 205–219.
Zheng, S., Sun, X., Song, X., Yang, Y., Ritzwoller, M.H., 2008. Surface wave tomography of China from ambient seismic noise correlation. Geochemistry Geophysics Geosystems 9, Q05020.
Zheng, X., Jiao, W., Zhang, C., Wang, L., 2010. Short-period Rayleigh-wave group velocity tomography through ambient noise cross-correlation in Xinjiang, Northwest China. Bulletin of the Seismological Society of America 100, 1350–1355.